

Power Management Regulation Control Integrated with Demand Side Management for Stand-alone Hybrid Microgrid Considering Battery Degradation

Ramy Adel Younis *‡, Doaa Khalil Ibrahim **, Essam M.Aboul-Zahab ***, Aboul'fotouh El'Gharably*****

*Department of Electrical Power & Machines, Higher Institute of Engineering at El-Shorouk City, Cairo, Egypt

**Department of Electrical Power Engineering, Faculty of Engineering, Cairo University, Giza, Egypt

*** Department of Electrical Power Engineering, Faculty of Engineering, Cairo University, Giza, Egypt

****Department of Electrical Power & Machines, Higher Institute of Engineering at El-Shorouk City, Cairo, Egypt

(ramy.younis.9@gmail.com, doaakhalil73@gmail.com, Zahab0@yahoo.com and a.abdelreheem@sha.edu.eg)

‡

Corresponding Author; Ramy Adel Younis, Higher Institute of Engineering at El-Shorouk City , Cairo, Egypt, Tel: +20201006286463, ramy.younis.9@gmail.com

Received: 30.09.2019 Accepted:25.10.2019

Abstract- A new Power Management Regulation Control (PMRC) integrated with Demand Side Management (DSM) strategies is proposed to enhance the Energy Management System (EMS) of a stand-alone hybrid microgrid. The microgrid combines Wind and PV systems as Renewable Energy Sources (RES) with a hybrid Energy Storage System (ESS) of Battery and Fuel Cell/Electrolyzer set. Towards achieving Net Zero Energy Supply, such microgrid is adequate in remote and isolated new communities with AC controllable critical and noncritical loads. The proposed PMRC implies two-levels of control based on Multi-Agent System (MAS). The first level keeps the output power of each source in its maximum available output power by applying maximum power point tracking (MPPT) techniques. The second level is based on making proper decisions for achieving the power balancing regulation and coordination between the available and the reserve power of the RES and ESS under different operating modes. Valley Filling, Energy Conservation and Load Shifting are applied as DSM strategies to improve loads sustainability during system contingencies. Considering the battery as the most expensive part in the microgrid, the effectiveness of the proposed strategy is further verified by determining the maximum permissible estimated battery lifetime during the operation in all possible scenarios. Extensive simulation studies for various scenarios of microgrid operation in a year were carried out using Matlab/ Simulink with realistic typical wind speed, solar irradiation data and restricted by the status of available ESS.

Keywords: Battery lifetime estimation, Demand Side Management (DSM), Energy Management System (EMS), Energy Storage System (ESS), Multi-Agent System (MAS), Power Management Regulation Control (PMRC), Renewable Energy Sources (RES).

1. Introduction

According to the International Energy Agency Report [1] in 2017, around 1 billion of people live without electricity access in remote and rural isolated communities in all over the world. In such areas, diesel generators are commonly used because of their reliability, smooth starting and low installation cost. Due to the great concern about the global warming, the issue of global CO₂ emissions from fuel combustion has grown in importance; such global emissions in 2016 were 32.31 GT [1]. On the other hand, the utilization of Renewable Energy Sources (RES) presents significant environmental benefits; however the extracted power from RES cannot meet the continuous variations of the load conditions because of the intermittent nature of wind speed, continuous variation of solar irradiation and temperature. Integrating different renewable energy systems that is called Hybrid Power System (HPS) and applying Energy Storage System (ESS) are essential solutions to ensure more continuous and reliable operation as discussed in [2-10].

Appropriate control and coordination strategy among various subsystems of HPS is the main challenge facing HPS performance [11,12]. Besides, when the microgrid operates in stand-alone mode, an adequate load sharing mechanism is required to equipoise the sudden changes in available power. Many efforts have been exerted and reported in literature to focus on various issues of HPS in islanded mode such as the size and cost optimization [13-15].

Several other studies have discussed the power quality and reliability issues of HPS as in [16-17]. The optimal batteries usage with different energy tariffs is investigated in [18] and similar work has focused on load shifting strategy through an optimal battery operation in [19]. Both studies have discussed the utilization of battery to enlarge the net profit of battery investment regardless of battery degradation. Battery degradation issue is considered in [20] where a high-resolution model is presented allowing for comparing different energy storage technologies. An approach including two models: economic and degradation models are presented in [21] as an iterative approach for optimal operation of PV systems; however no sensitivity analysis is performed to identify the level of degradation allowed for the technology to become cost competitive.

Despite of the enormous advantages of Energy Management System (EMS) in islanded microgrids, there are also some constrains that affect their performance such as the limited power generation, restricted energy storage and fuel cost. Limited power generation can cause brownouts, due to peak demands; resulting in lack of reliability and making some loads stop proper working as pointed out by [22,23]. Consequently, there is a strong motivation to apply Demand Side Management (DSM) in reducing load or spreading load over time ensuring that electricity is equitably shared among the microgrid users. Multi-agent system (MAS) has become the most widely approach used for EMS in microgrids, where each agent is intelligent and able to communicate with its neighboring agents to form a larger intelligent entity [24].

From all of the aforementioned research studies, it appears that, as yet, there is a little attention has been paid to develop a comprehensive management of stand-alone microgrid under inadequate energy reserves during contingencies that may lead to entire system blackout. For isolated microgrids, the potential of DSM besides the EMS is worthy to be considered to improve loads sustainability while minimizing the consumption costs, and also enhancing the ESS life time.

Achieving a comprehensive coordination management in the presence of hybrid RES and hybrid ESS considering battery degradation incorporated with DSM strategies applied to the end-users can be regarded as one of the most promising solutions to maintain the sustainability of loads as long as possible. The aim of this study is to present a scheme that addresses different issues simultaneously. It takes the form of a case-study of stand-alone hybrid RES microgrid located in isolated community. The studied microgrid is supplied by a Net Zero Energy Supply combining two renewable energy sources consisting of a PV array and a permanent magnet synchronous generator (PMSG) wind turbine and a hybrid ESS including battery units and fuel cell/Electrolyzer set. AC loads connected to the studied microgrid are controllable and categorized based on priority level as critical and noncritical loads. This paper aims to contribute to the growing area of research for providing proper EMS by implementing a new integrated power management regulation control (PMRC) with DSM strategies. The applied PMRC strategy is accomplished based on two-levels of control using MAS. The *first level* uses the dynamic operating points of each subsystem for extracting maximum power available under varied range of environmental weather conditions. Artificial intelligent control is applied for PV MPPT, the battery storage units operate in voltage control mode to maintain constant DC link controlled by a bidirectional dc-dc converter, while the fuel cell operates in power control mode controlled by the hydrogen flow regulator and boost converter. The *second level* depends on making appropriate decisions for power balancing regulation and HPS coordination to meet load requirements variations under different operating modes, and also utilizing load shedding power regulation control to maintain the sustainability of

loads, as long as possible, under system contingencies based on predetermined priority levels. To further enhance the EMS by improving the sustainability of loads and minimizing consumption costs to some of the end-users, DSM programs such as Valley Filling, Energy Conservation and Load Shifting strategies are implemented under different operating modes of Excess Power of Primary Source mode (EPPS) and Load Shedding mode (LSM). The performance of the proposed system has been extensively tested under different wind speeds, solar irradiation and load conditions. The achieved results show the potential ability of the proposed scheme and confirm its effectiveness.

2. Configuration of Tested Isolated Microgrid

The tested microgrid is configured as depicted in Fig. 1. It is composed of: KYOCERA KC 200 GT 100 kW solar array PV system, ZENIA Energy 30 kW PMSG wind turbine generating system, Proton Exchange Membrane Fuel Cell (PEMFC) stack integrated with its electrolyzer and hydrogen storage tank and Lithium-ion (Li-ion) battery units.

The connected load to the tested system in Zafarana, Egypt has been considered based on the Canal Company for Electrical Distribution (CCED) Suez Sector [25], with reduced scaled values. The load varies between minimum and maximum values during typical day. Basically, Zafarana site is divided into residential and industrial regions. The residential region comprises three tourist villages, a hospital, a police station, a bank and also some water pumping loads for the landscape areas for villages. While the industrial region comprises several heavy industries such as steel and cement industries and light industries such as food processing and packaging industries. To simulate the complete tested microgrid in MATLAB/Simulink program, scaled loads are applied, as illustrated in Table 1, with different priority levels (from 1 to 9, where 1 denotes the highest priority which has been assigned to the hospital and heavy industries either steel or cement).

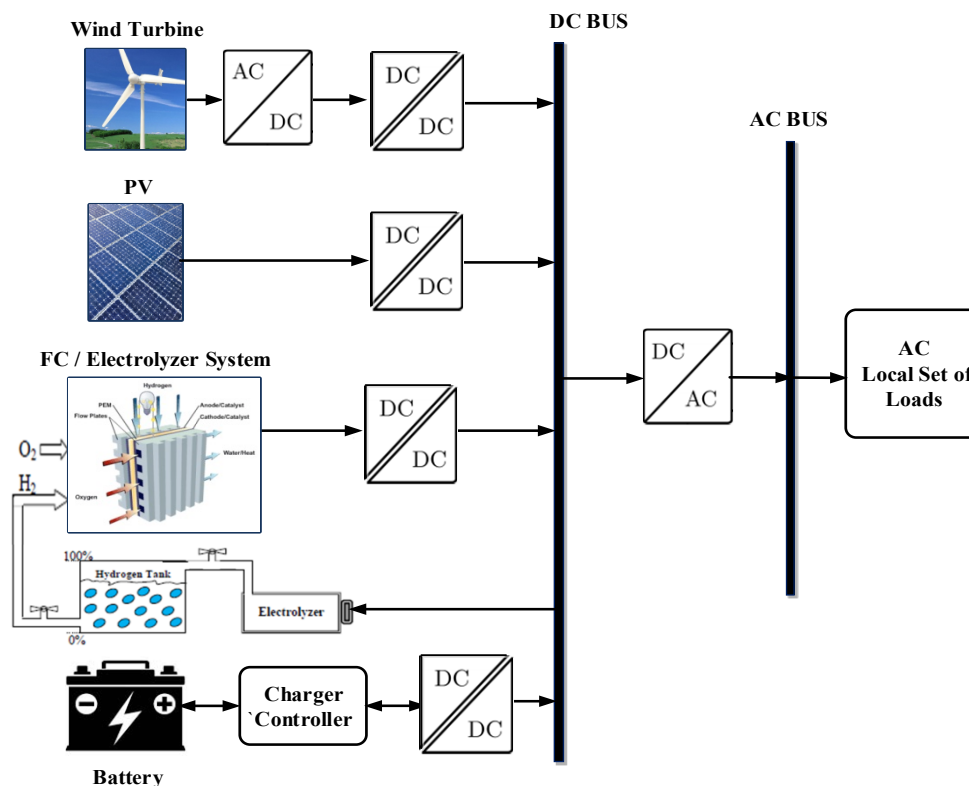


Fig. 1: Configuration of the tested microgrid

Table 1: Summarized loads of tested microgrid

Load Type	Load Serial	Load Description		Priority Level	Min. Registered Load Value (kW)	Max. Registered Load Value (kW)
Residential	L1	Hospital	Services	1	15	25
	L4-1A	Tourist Village 1	Air conditioning	7	10	25
	L4-1B		Lighting & services	4		
	L4-2A	Tourist Village 2	Air conditioning	8	10	25
	L4-2B		Lighting & services	5		
	L4-3A	Tourist Village 3	Air conditioning	9	10	25
	L4-3B		Lighting & services	6		
	L3	Police Station	Services	3	10	30
L3	Bank	Services	3			
Industrial	L2-1	Steel Industry	Heavy Industry	1	25	35
	L2-2	Cement Industry	Heavy Industry	1	25	30
	L2-3	Food Industries	Light Industry	2	10	25
Total Loads (kW)					115	220

2.1 Site Characteristics

Such microgrid is located in Zafarana site in the Suez Gulf area that lies on the East coast of Red Sea zone in Egypt at latitude and longitude angles of 32' 36" and 29' 06" respectively. Distinctive features of Zafarana site have been collected from NASA Modern-Era Retrospective Analysis for Research and Applications (MERRA) for a typical year from the interval of 1st November 2017 to 31st October 2018 [26]. The measured wind speed (velocity V_1 at Z_1 lower altitude) is modified according to turbine hub height and corrected for the typical operation (velocity V_2 at Z_2 higher altitude) based on: $V_2 = V_1 \cdot (\frac{Z_2}{Z_1})^\alpha$, where α is the shear exponent, that depends on the landscape type; it usually equals 0.423 for villages, agricultural lands with many or tall sheltering hedgerows, forests and very rough and uneven terrain [27].

A detailed monthly and annual analysis for the wind speed and solar radiation-temperature data at Zafarana site for the year starting at Nov. 2017 is carried out and tabulated in Table 2. In which, wind speed and solar radiation are classified into four ranges (*Zero, Low, Medium and High*) according to assumed boundaries. The table demonstrates

the No. of hours for each range in every month and in the whole year. Basically, the studied year has included typical normal and abnormal weather conditions with different ranges for wind speed and solar radiation. It has been noticed that the No. of hours per month that the wind speed falls in the *Zero* range was dominant at December 2017 compared to August for the prospective year, however the No. of hours of *High* wind speed range was in September 2018 compared to July for the same year. While the *High* radiation solar range was recorded in June and July 2018, whereas the *Zero* solar radiation was documented in December 2017.

Actually, the status of RES in the tested site along the year can be summarized in four scenarios and therefore the proposed PMRC strategy will be designed to deal with the following scenarios:

- Scenario No. 1 designates High wind/High radiation (HWHR);
- Scenario No. 2 designates Medium wind/Medium radiation (MWMR);
- Scenario No. 3 designates Low wind/Medium radiation (LWMR);
- Scenario No. 4 designates Zero wind/Zero radiation (ZWZR) with/without DSM.

Table 2: Monthly and annual analysis in Zafarana site from Nov. 2017 to Oct. 2018

Month	No. of Hours							
	Ranges for Wind Speed				Ranges for Solar Radiation			
	Zero (0-3 m/s)	Low (3-5 m/s)	Medium (5-9 m/s)	High (over 9 m/s)	Zero (0-100 w/m ²)	Low (100-200 w/m ²)	Medium (200-500 w/m ²)	High (over 500 w/m ²)
Nov. 2017	56	165	439	60	444	39	96	141
Dec. 2017	234	186	266	58	489	39	146	70
Jan. 2018	54	188	416	86	468	32	105	139
Feb. 2018	212	203	218	39	405	44	96	127
Mar. 2018	112	227	339	66	424	26	91	203
Apr. 2018	91	185	366	78	384	38	79	219
May 2018	117	177	388	62	380	44	100	220
June 2018	49	138	425	108	360	23	87	250
July 2018	23	211	462	48	372	29	93	250
Aug. 2018	3	74	564	103	374	41	82	247
Sep. 2018	11	65	530	114	398	26	85	211
Oct. 2018	67	114	492	71	435	40	98	171
Total No. of Hours	1029	1933	4905	893	4933	421	1158	2248
	8760				8760			

2.2 Battery lifetime estimation

Li-ion battery model is developed according to the generic model introduced in [28], while its controller is a bidirectional dc-dc converter that stabilizes the dc link voltage during sudden changes. Actually every charging and discharging cycle the battery performs; it loses a portion of

its capacity and power capability that is called ageing or degradation. Different factors affect battery degradation such as time, number of cycles, temperature, State of Charge (SOC), and cycle depth. For a complete comprehensive vision for the management strategy of the overall system, it is anticipated to determine the no. of replacements of

the battery during the lifetime of the project; consequently the battery lifetime estimation based on the discharge pattern is considered the most significant part in the complete management strategy as proposed in this paper. In fact, different techniques are proposed in several researches but most of them suffer from some shortcomings as they require detailed information about battery performance and being complicated and time consumed as in [29-31] while some other techniques are only valid for certain type of battery as in [29, 30].

In this paper, in order to avoid further battery degradation, the battery should not be overcharged or exposed to severe charging or discharging events and should follow the limitations on State of Charge (SOC) as given in Eq.(1) and (2).

$$SOC_{min} \leq SOC(t) \leq SOC_{max} \quad (1)$$

$$i_{max_charge} \leq i(t) \leq i_{min_discharge} \quad (2)$$

Where SOC_{min} , SOC_{max} present the minimum and maximum allowable state of charge respectively, while i_{max_charge} , $i_{min_discharge}$ define the maximum charging and minimum discharging current of battery. As well known, the battery life decreases with the increase in Depth of Discharge (DOD) described in Eq. (3).

$$DOD = 1 - SOC \quad (3)$$

In the applied technique for battery lifetime estimation, varying depths of discharge and varying rates of discharge are considered. Basically, the applied battery lifetime estimation is based on the following three assumptions [32]:

1: The cell has a finite life as it will end up when the cumulative effective amp-hour (Ah) corresponding to series discharge events equal to life of cell as given in Eq. (4).

$$\Gamma_R = L_R D_R C_R \quad (4)$$

Where Γ_R is the Ah life of a cell under actual operating conditions, L_R is the cycle life at rated depth of discharge and rated discharge current, D_R is the percentage depth of discharge at which rated cycle life was determined and C_R is the Ah capacity of a cell at rated discharge current.

2: The actual charge life of cell is a function of DOD, therefore the effective Ah discharge in a given discharge event may be more or less than the actual discharge D based on actual DOD. This assumption deals with performing a best fit of the following expression.

$$L = u_1 \left(\frac{D_R}{D}\right)^{u_0} \times \exp\left(u_2 \left(1 - \frac{D}{D_R}\right)\right) \quad (5)$$

These three parameters u_0 , u_1 and u_2 represent coefficients of the DOD fitting function. They provide considerable flexibility in fitting to manufacturer data and give reasonable life cycle vs. DOD relationship even with very few given data points.

3: The life of cell Γ_R drops whenever the cell is discharged faster than the rated rate, therefore the effect of discharge rate (d_{eff}) will be estimated using a simplified form that depends on actual Ah discharge d_{act} and actual Ah capacity of battery C_A as in Eq. (6).

$$d_{eff} = \left(\frac{C_R}{C_A}\right) \times d_{act} \quad (6)$$

Finally, in order to estimate battery lifetime which has been exposed to series of discharge rate patterns (n) in time period T corresponding to the series of discharge events, the accumulative effective discharge can be calculated as follows:

$$L_{time} = \frac{L_R D_R C_R}{\sum_{i=1}^n d_{eff,i}} \times T \quad (7)$$

In this study, the Intensium Max Li-ion battery from SAFT Company [33] is considered as a storage device, the cycle life of battery is plotted against DOD of the battery as illustrated in Fig 2.

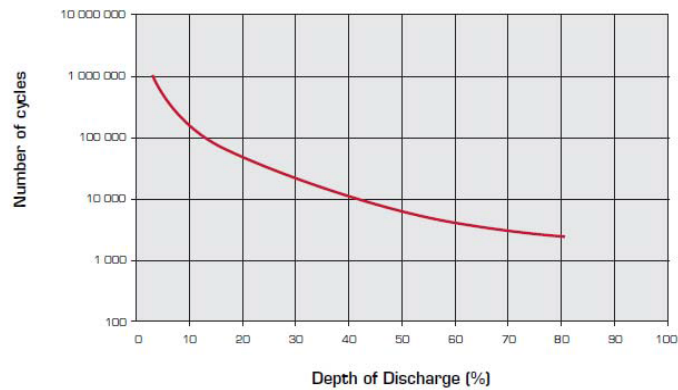


Fig. 2. Cycle life vs. DOD for high energy Intensium Max Li-ion battery based on SAFT Company

3. Energy Management System of the Tested Microgrid

As mentioned before, a new integrated PMRC incorporated with DSM strategies is implemented for achieving a comprehensive EMS. The PMRC relies on two-level control based on MAS as illustrated in Fig. 3. The structure of the MAS is developed using five agents: 1st Agent for PV system, 2nd Agent for wind energy conversion system, 3rd Agent for fuel cell system, 4th Agent for Li-ion battery system and 5th Agent for the load.

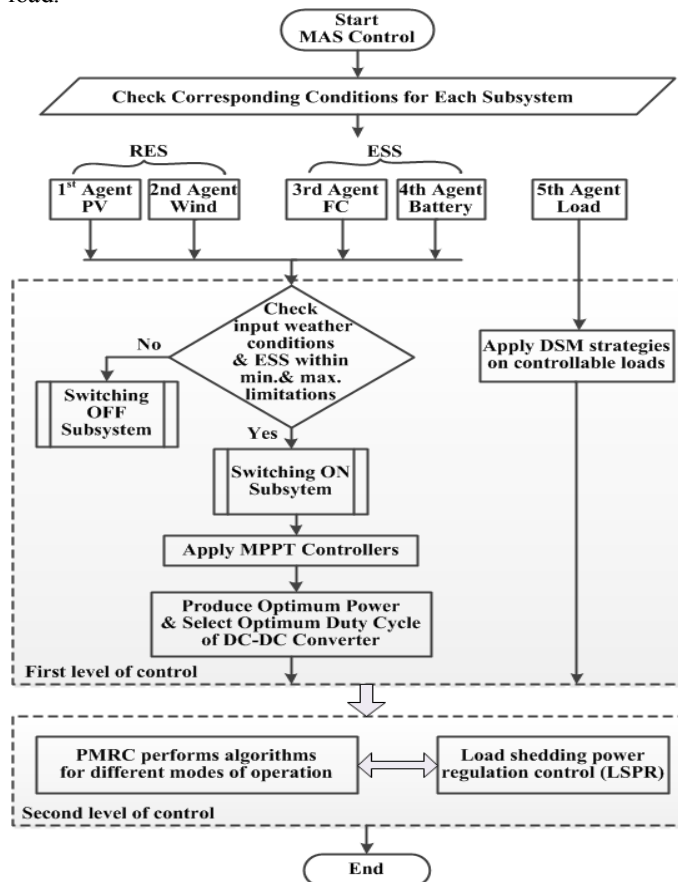


Fig. 3: Two-level control for EMS using MAS

The first level of control is responsible for the internal switching controls for each subsystem in the overall system and each subsystem checks the input corresponding conditions (solar irradiation and temperature for the 1st Agent, wind speed for the 2nd Agent, hydrogen pressure for the 3rd Agent and the SOC limits for the 4th Agent), while the coordinated switching controls for operational mode are implemented through the second level control. Both PV and wind energy conversion systems are controlled by boost converters in order to extract optimum power by applying MPPT techniques. These two agents (1st Agent and 2nd Agent) receive the solar irradiation, temperature and wind speed data and then send signals to PV & wind turbine breakers to close when this data is within the nominal predetermined range, and also apply

the MPPT technique to produce the appropriate duty cycle for the boost converter.

The algorithm for FC agent (3rd Agent) works out when the hydrogen tank pressure is above its minimum value, thus the MPPT technique is applied and sends an appropriate duty cycle to the boost converter to produce power from the FC while the FC breaker opens when the hydrogen pressure level is below the minimum limit. The objective of the battery agent (4th Agent) is responsible for charging and discharging the battery according to available power and load variations. Such agent drives the duty cycle command to the boost converter and switches off the battery in case of overcharging or when SOC reaches the minimum allowable level. In fact, the battery is controlled by a bidirectional dc-dc converter, while the FC system is controlled by the hydrogen flow regulator and boost converter.

Actually, the PMRC implies the actual recorded weather conditions (wind speed, solar irradiation and temperature data) for a specific period of time and also initializes SOC and the hydrogen pressure status based on MAS for each subsystem and the first level of control. In this paper for normal operating conditions, the hydrogen pressure $H_{2\text{press}}$ is within maximum ($H_{2\text{press max}}$) and minimum ($H_{2\text{press min}}$) allowable limits, which are taken by 0.0001 and 0.04 MPa for a tank of 1 cubic meter volume. While the battery SOC is kept within nominal (SOC_{nom}) and maximum (SOC_{max}) permissible boundaries of 70% to 90% respectively [34], however, it should be noted that the SOC is allowed to be as low as 60% ($SOC_{min_critical}$) for only critical operating conditions. DSM strategies are implemented on the load (5th Agent) to optimize energy consumption and maximize the end-users efficiency.

In the second level, the PMRC controller takes corresponding decisions by closing and opening the agents' breakers to meet load demand. It is constructed to achieve the power balance in every operating state, maintain battery SOC and the hydrogen pressure within acceptable limits, and provide the minimum limit for sustaining critical loads as much as possible according to the priority of shedding during contingencies.

3.1 Second Level Methodology of PMRC

The proposed PMRC strategy is implemented for the three possible modes of operation as depicted in Fig. 4; such modes are implemented against four different scenarios. Generally, the PMRC system confirms the sustainable operation of the microgrid system via online central dynamic programming through the coordination between the hybrid primary energy sources (wind turbine and PV system) and the hybrid storage system (battery and FC) with loads.

Based on weather conditions, load profile and the state of reserve for hybrid ESS, the proposed PMRC regulates the load profile that can be supplied from the system according to predefined priority levels. Accordingly, the power balance equation of the microgrid can be expressed as given in Eq. (8), where P_{RES} is the total power extracted from RES ($P_{RES} = P_{WIND} + P_{PV}$), P_{PV} is the PV power, P_{WIND} is the wind power, P_{FC} is the extracted power from fuel cell, while the electrolyzer absorbed power is denoted by P_{ELZ} and finally the battery power is expressed by P_{BAT} in which '-' indicates charging and '+' indicates discharging. The total load power is represented by P_{LOAD} for the summation of the four loads of the microgrid ($L1, L2, L3$ and $L4$) as shown in Eq. (9).

The PMRC system has to manage supplying the load within the allowable limits of all subsystems. When the wind and solar powers are high enough ($P_{RES} > P_{LOAD}$), represented by both scenarios No. 1 (HWHR) and No. 2 (MWMR), the total load is easily met and the excess

power (P_{EXCESS}) is consumed to charge battery and/or produce hydrogen by the electrolyzer (P_{ELZ}) according to Eq. (10). Such mode is the 1st Mode of operation, which is called "Excess Power of Primary Source (EPPS)" and its flowchart algorithm is described in Fig. 5.a. In fact, the battery is charged and/or the hydrogen is produced as long as the $SOC < SOC_{max}$ and the hydrogen pressure $H_{2\text{press}} < H_{2\text{press max}}$ and no power curtailment is done, otherwise the valley filling strategy is applied by supplying some other water pumping loads. As illustrated in Fig. 5.a, the PMRC system operates in EPPS mode within three possible operating states.

$$P_{RES} + P_{FC} \pm P_{BAT} = P_{LOAD} + P_{ELZ} \quad (8)$$

$$P_{LOAD} = \sum \text{loads power} = P_{L1} + P_{L2} + P_{L3} + P_{L4} \quad (9)$$

$$P_{EXCESS} = P_{RES} - P_{LOAD} = P_{ELZ} + P_{BAT} \quad (10)$$

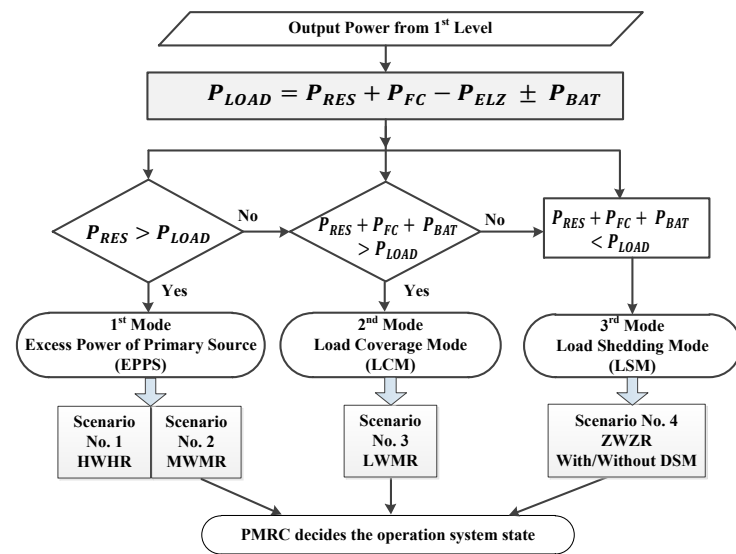
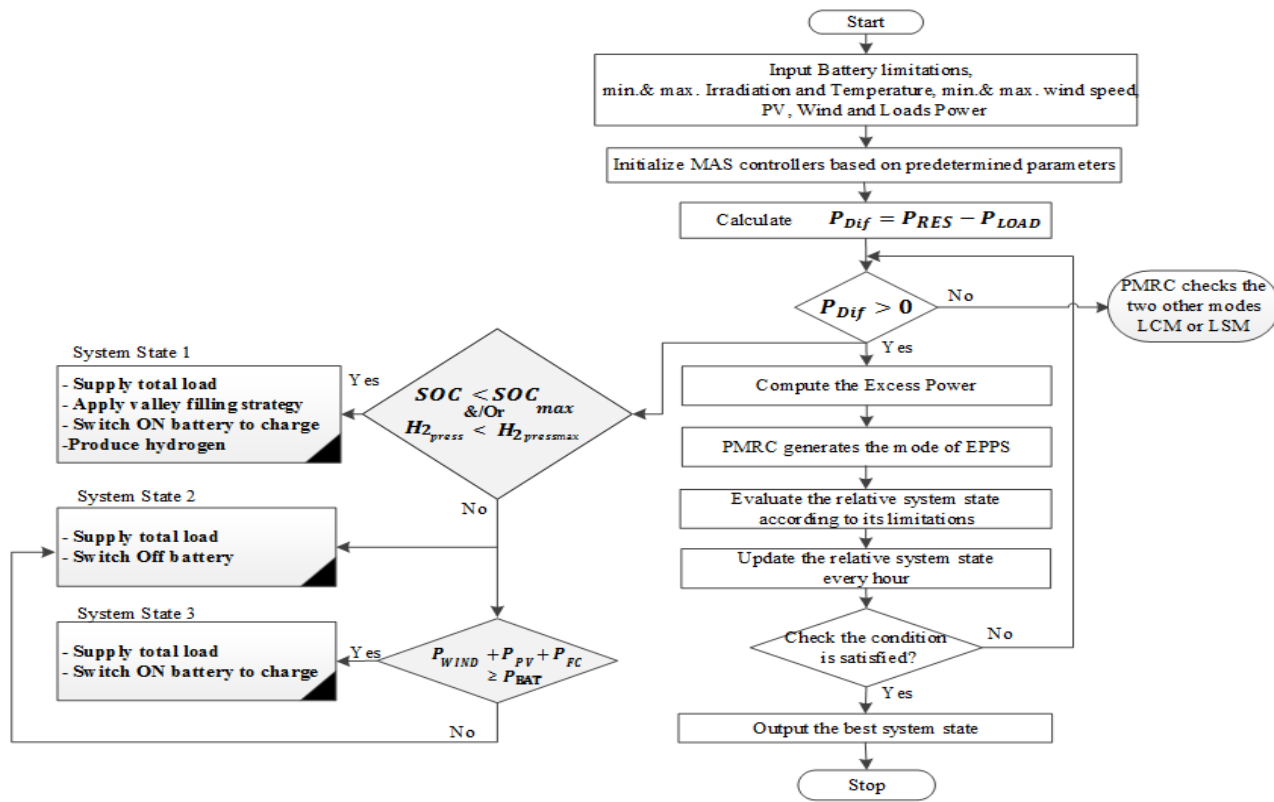


Fig. 4: Modes and scenarios for power management regulation control (PMRC)

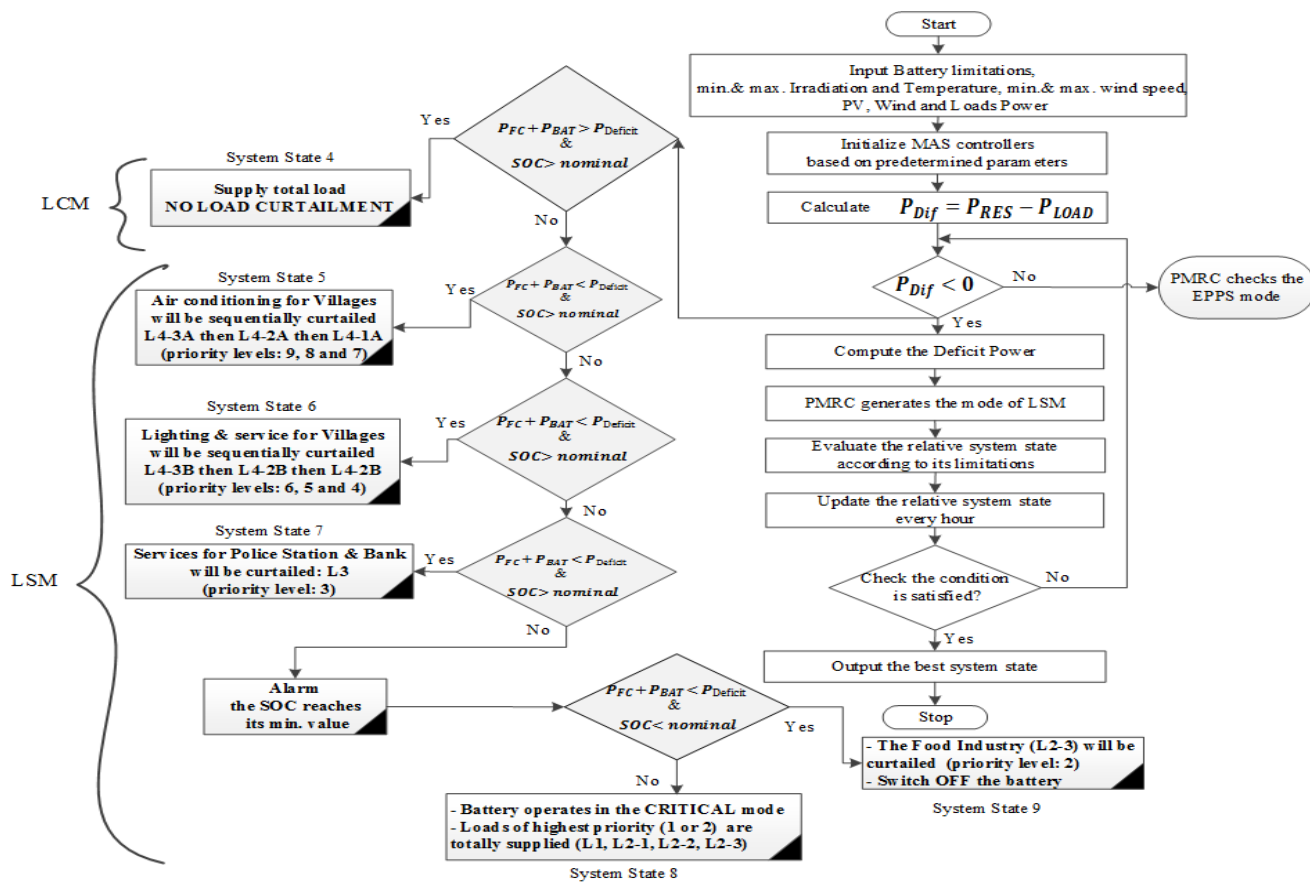
On the other hand, during low wind and solar conditions ($P_{RES} < P_{LOAD}$) as represented in scenario No. 3 (LWMR), the deficit power ($P_{DEFICIT}$) may be supplied from the fuel cell and battery storage by applying Eq. (11). Such mode may possibly be the 2nd Mode of operation, which is called "Load Coverage Mode (LCM)" or the 3rd Mode of operation, which is called "Load Shedding Mode (LSM)".

$$P_{DEFICIT} = P_{LOAD} - P_{RES} = P_{FC} + P_{BAT} \quad (11)$$

Such deficit power ($P_{DEFICIT}$) is checked against the possible supplied power from the hybrid ESS (summation of P_{FC} and P_{BAT}). In case that: $P_{FC} + P_{BAT} > P_{DEFICIT}$, the SOC is greater than SOC_{nom} and also the hydrogen pressure $H_{2\text{press}}$ is greater than the minimum value ($H_{2\text{press min}}$), the PMRC turns into LCM and no load curtailment occurs as the total deficit power ($P_{DEFICIT}$) is supplied from hybrid ESS. On contrary, when: $P_{FC} + P_{BAT} < P_{DEFICIT}$, or the SOC is greater than SOC_{nom} , that may be considered system contingency, the PMRC turns into LSM, and thus sequential curtailment for the less priority loads are carried out with/without applying DSM strategies that is covered in scenario No. 4 (ZWZR). The flowchart of the algorithm for both LCM and LSM modes is described in Fig. 5.b.



a) EPPS operating system states



b) LCM and LSM operating system states

Fig. 5: Flowcharts for different operating system states

The PMRC then decides the operation system state based on the input weather data, load conditions and actual limitations of all subsystems. As illustrated in the flowcharts of Fig. 5.a and Fig. 5.b, the operation system states are distinguished into 9 states. For states 1 and 3, the battery is switched ON to charge, while it is switched OFF in state 2 during EPPS mode. During LCM and LSM, the battery discharges for operation system states 4, 5, 6 and 7, till reaching $SOC_{min_critical}$ at state 8, and finally switched OFF at state 9. From load point of view, the total load demand is met during systems states

of 1 to 4 (EPPS & LCM), while the load demand is partially met according to priority level during systems states from 5 to 9 (LSM).

3.2 Applied Demand Side Management Strategies

Actually, proper energy management can enhance loads sustainability. It is anticipated that reducing load or spreading load over time ensures that electric energy is appropriately shared among microgrid customers. This type of energy management is entitled Demand Side Management (DSM). In fact, the implementation of such

strategies can bring significant cost benefits to energy end-users and a reduction in carbon emissions, furthermore, some measures to apply DSM are not necessarily expensive, and may even be free of charge, and often easy to implement in developing areas [35].

DSM strategies have different classifications [35], this study follows three strategies those namely: load shifting, energy conservation and valley filling as illustrated in Fig. 6.

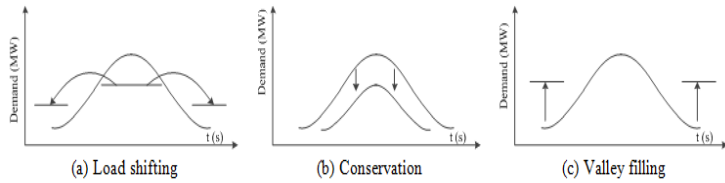


Fig. 6: Applied DSM strategies

Load shifting strategy, shown in Fig. 6-a), reduces the energy consumption of the daily peak period without having to limit the usage of appliances as the load is transferred to lower demand periods, however, the consumers are obliged to change their activities [35]. Such strategy can be implemented effectively on some shiftable controllable heavy loads as described in Table 4. Implementing load shifting strategy for $P_L(t)$ is modeled by adding shifting factor $S_L(t)$ that is enhanced by the EMS. Therefore, the expected load $\tilde{P}_L(t)$ can be expressed by [36]:

$$\tilde{P}_L(t) = S_L(t) \times P_L(t) \quad (12)$$

This shifting factor $S_L(t)$ in time t is bounded by time dependent constraints as the response of a DSM would vary in different periods of the day as follows:

$$S_{Lmin}(t) \leq S_L(t) \leq S_{Lmax}(t) \quad (13)$$

For example, when $S_{Lmin}(t)$ equals 0.9, it means that consumers can reduce a maximum of 10% of their expected load in each time step. Similarly, when $S_{Lmax}(t)$ is 1.1, it is clear that consumers can only increase a maximum of 10% of their expected load.

The first important feature for load shifting is to decide the total number of shifting steps (N_{Ts}) [37], this can be determined by shifting duration and shifting increment at every time step (n_{incr} which is specified by the users), as expressed in Eq. (14):

$$N_{Ts} = \frac{\text{shifting duration}}{n_{incr}} = \frac{|t_{end} - t_{start}|}{n_{incr}} \quad (14)$$

The shifting duration is determined by two variables: start time (t_{start}) and end time (t_{end}) and differs on each other based on whether the maximum negative and positive shifting steps are defined, assuming that the controlled period is specified from θ to T , T is the end of the whole control period. Thus, the total demand at each shifting increment step is determined using Eq. (15), which sums up all the sub-demands after the load shifting at certain time as follows:

$$\text{new}\tilde{P}_L(t) = \sum_{j=1}^n P_L[j](t) \quad (15)$$

Where n denotes the total number of demands, $\text{new}\tilde{P}_L(t)$ presents the new total demand at time step t ; and $P_L[j](t)$ is the j th demand profile after being shifted at time step t .

The goal of applying energy conservation strategy, shown in Fig. 6-b), is to decrease the entire daily load, by using efficient A++ appliances and electric equipment or even by raising customers' awareness to have more concern for the use of energy. Exchanging incandescent light bulbs by compact fluorescent light bulbs is one of the most known examples of energy conservation strategy as mentioned in [22] and [38]. Such strategy is implemented effectively on some loads as described in Table 3.

Finally, valley filling strategy, illustrated in Fig. 6-c), aims to built-up energy demand during off-peak periods to smooth out the load and improve the economic efficiency of the microgrid. Valley filling is considered for decreasing the waste of energy produced during the EPPS mode. As clearly shown in Table 3, it is implemented effectively by adding two scaled loads: water pumping irrigation for landscape areas and swimming pools.

DSM strategies can be implemented with some measures and technologies, actually technologies are usually more expensive solutions than DSM measures, since they require the purchase of equipment [22]. Three examples for encouraging load management are recommended to be applied in this study: 1) using efficient appliances and lighting systems, 2) applying prices incentives and tariffs structure for load scheduling, and 3) consumer awareness and community involvement. Furthermore, some technologies are recommended to apply DSM in this study: smart current limiters, distributed intelligent load controllers, prepaid meters and advanced metering systems with centralized communication.

Table 3: Loads that follow DSM strategies

DSM Strategy	Load Area	Loads			
Load Shifting	Hospital & Tourist Villages	Main Laundry	Washing machines	Main Kitchen	Dish washer
			Dryers		Oven, Kettle, Toaster
			Electric irons		Blender and Coffee maker
	Police Station & Bank	Water dispenser, kettle, oven, coffee maker, fans, and small fridges.			
Energy Conservation	Hospital	Lighting, heating system, mechanical ventilation and HVAC.			
	Tourist Villages	Indoor & outdoor lighting, washing machines and fridges.			
	Police Station	Lighting and some small loads.			
Valley Filling	Tourist Villages	Water pumping irrigation for landscape areas.			
		Water pumping for swimming pools.			

4. Simulation Results for the Proposed System

To show the potential ability of the proposed scheme, the case study system has been extensively tested under realistic data. The behavior of proposed scheme is observed for the three possible modes (EPPS, LCM and LSM) under changing environmental and load conditions. Some distinctive days are adequately selected (four days) to covers the **four scenarios** for the **three modes of operation** as follows:

- Day 1: 8th of June 2018 representing High wind/High radiation (HWHR); it characterizes scenario No. 1.
- Day 2: 16th of January 2018 representing Medium wind/Medium radiation (MWMR); it characterizes scenario No. 2.

- Day 3: 5th of December 2017 representing Low wind/Medium radiation (LWMR); it characterizes scenario No. 3.
- Day 4: 28th of December 2017 representing Zero wind/Zero radiation (ZWZR); it characterizes scenario No. 4 with and without applying DSM.

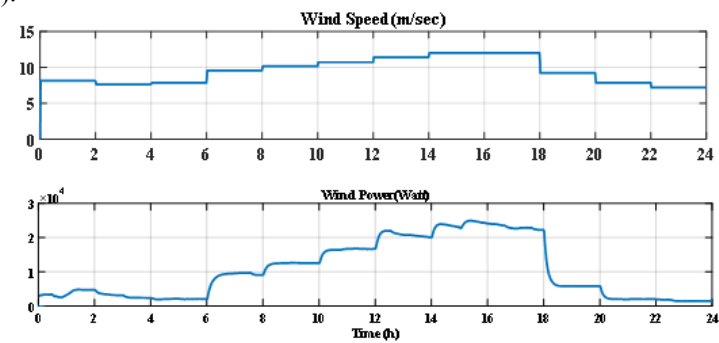
Actually, the recorded weather data for these four typical days cover the whole year of study. They are almost repeated seasonally over the year within same specified ranges for classifications and so they are selected as inputs for the simulated system with its MAS controllers. Therefore, the proposed PMRC algorithm determines the mode of operation as explained before. In the following subsections, the performance of the local controllers under variation of load profile is

simulated by the PMRC, hence determining the operating states according to each mode.

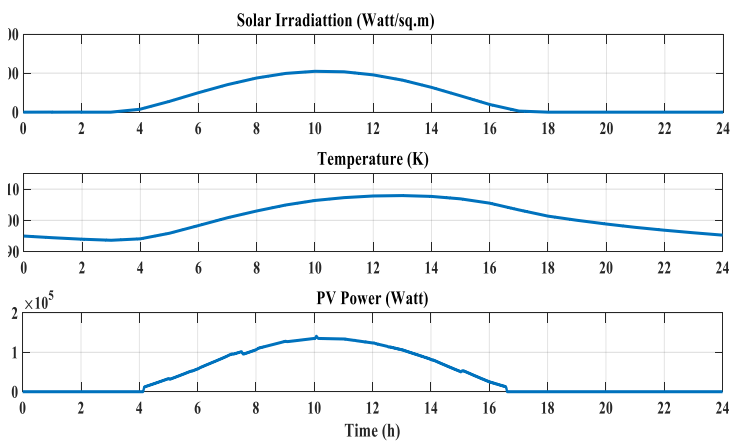
4.1 Results for EPPS mode at Day 1 covering scenario No. 1 (HWHR)

The case of high wind speed with high irradiation is adopted in that mode. Fig. 7.a shows the variation of wind speed and the corresponding output power over the 24 hours of Day 1 (8th of June 2018), also the solar irradiation and temperature and output PV power variation is presented in Fig. 7.b.

As shown in Fig. 8.a, at the time from 00:00 to 06:00 the power generated by the wind and FC is greater than the demand load and there is an excess power which can be utilized to charge the battery till reaching 88%. Also from 10:00 to 14:00, the PV power is increased as well as the wind power and the battery is recharged as shown in Fig. 8-b).



(a) Wind speed and output wind power

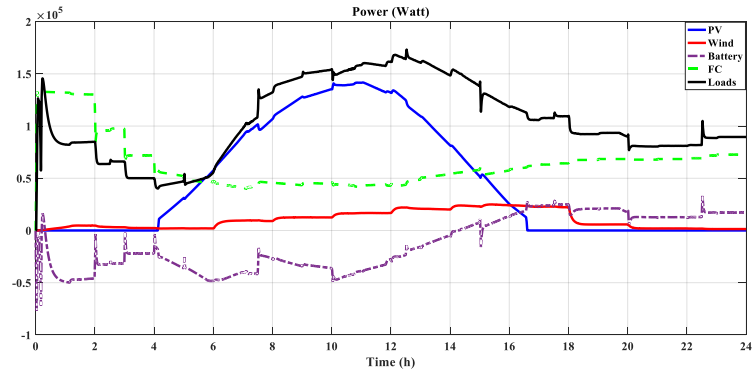


(b) Solar irradiation, temperature and output PV power

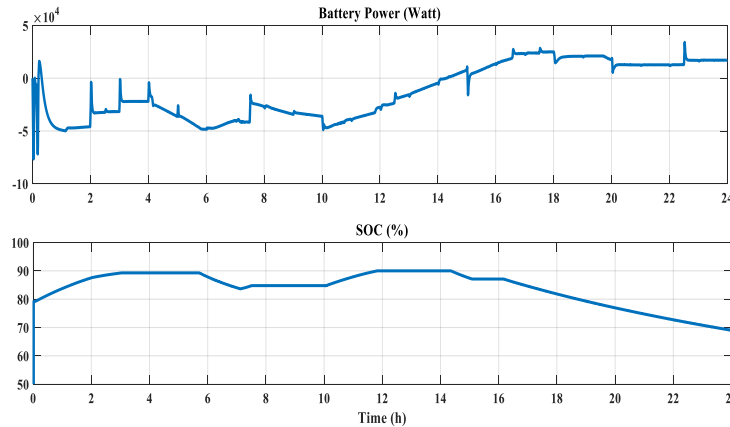
Fig. 7: Weather conditions and corresponding renewable output power through Day 1 covering scenario No. 1 (HWHR)

Figure 8-c) verifies the power balance as it shows three curves. The first curve describes the summation of generated power from sources: P_{PV} , P_{WIND} and P_{FC} , the second demonstrates the summation of consumed power from loads and the electrolyzer. This difference will be the third curve which denotes the battery power that will be added to generation in some intervals (discharging with -ve sign for power flow) and consumption in other intervals (charging with +ve sign for power flow).

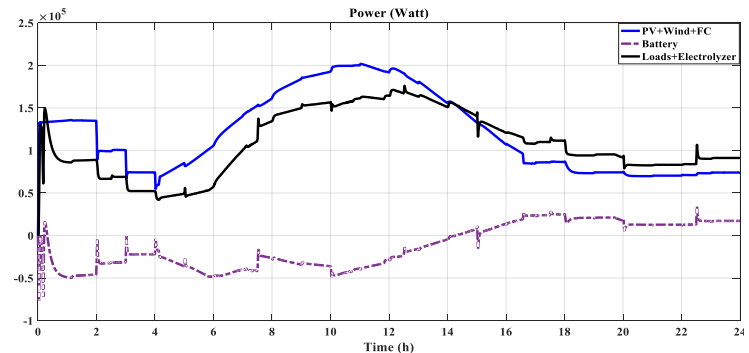
Due to the sequential alternating between charging and discharging events, the no. of battery cycles increases significantly over a complete day which results in fast aging of the battery. At 06:00 and 10:00 the difference in the power available can be utilized in connecting the prescribed valley filling load with a value of about 5 kW that is considered the reasonable sizing for the studied system as illustrated in Fig. 9. It is clear that the step or cyclic changes in the heavy loads of L2 and L4 that occur over the 24 h will result in some spikes compared to the unnoticeable spikes in L1 and L3.



a) Power trends including wind power, PV power, battery and FC with total load profile



(b) Output battery power and corresponding SOC



(c) Comparing generated power of PV, Wind & FC versus consumed power of Loads & Electrolyzer

Fig. 8: Generated and consumed power with the battery performance through Day 1 covering scenario No. 1 (HWHR)

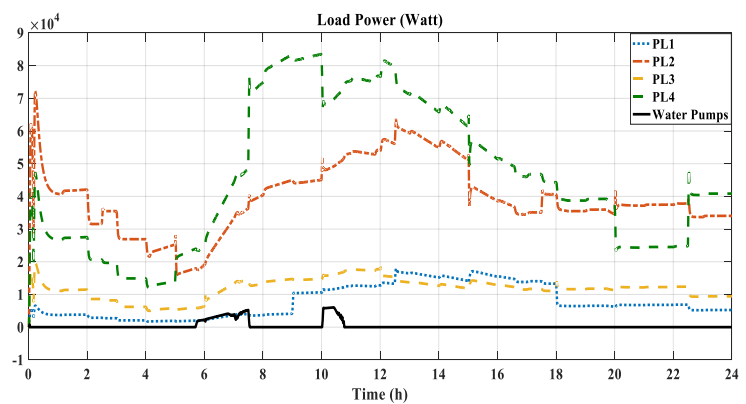


Fig. 9: Load profile with valley filling load through Day 1 covering scenario No. 1 (HWHR)

As deduced, the PMRC receives the input weather signals based on the MAS that in turn provides the MPPT operation of each subsystem hence the PMRC determines the operating mode. Accordingly, EPPS is completely verified at this scenario.

4.2 Results for EPPS mode at Day 2 covering scenario No. 2 (MWMR)

Day 2 (16th of January 2018) covers scenario No. 2 (MWMR). In that case, the wind speed and solar radiation ranges for most of the day lie in the medium range of the predefined classification. Thus, the excess power available from the RES for the day interval time is sufficient to charge the battery for particular hours and also the available excess in power can also be utilized for connecting the valley filling load. Therefore, the PMRC successfully achieves the EPPS mode verifying its operating system states.

4.3 Results for LCM mode at Day 3 covering scenario No. 3 (LWMR)

Day 3 (5th December 2017) covers scenario No. 3 (LWMR), in which LCM is activated. It verifies the robustness of the multi controllers subsystems, when the power supplied by hybrid RES is not sufficient to meet all load demand requirements along the 24 hours while the hybrid ESS is within its operational boundaries and can cover the unmet loads requirements without any curtailment, as illustrated in Fig. 10, from 00:00 to 04:00 and from 16:00 to 24:00. As shown, at the time of 15:00 when the load profile has decreased to about 120 kW, the FC power is sufficient to supply most of the deficit power and the battery controller has reduced its power to save its life time according to the PMRC algorithm.

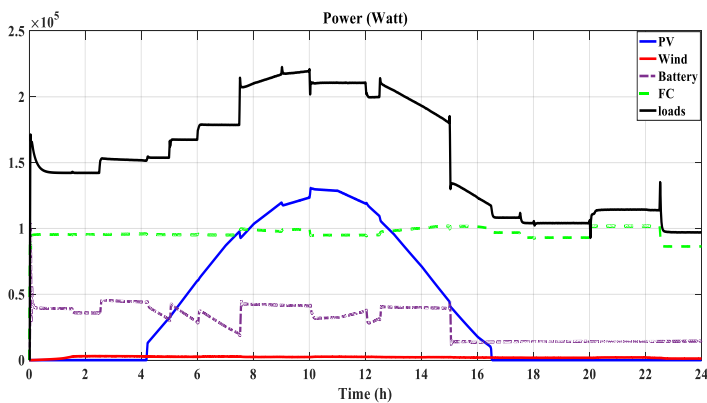


Fig. 10: Generated power trends including wind power, PV power, battery and FC with total load profile through Day 3 covering scenario No. 3 (LWMR)

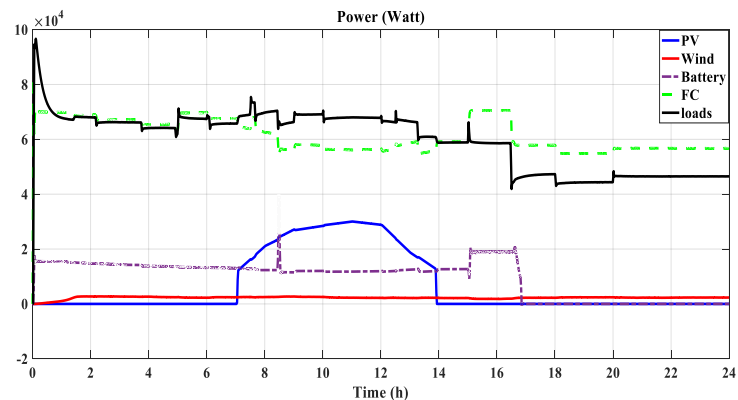
4.4 Results for LSM mode at Day 4 covering scenario No. 4 (ZWZR) without applying DSM

Two cases in scenario No. 4 for zero wind/zero radiation (ZWZR) may occur in the LSM mode, where complete contingency of the system has been adopted in this study during Day 4 (28th of December 2017). According to Table 2, a low wind speed with low solar irradiation is considered in that day. The PMRC algorithm checks the status of hybrid ESS (FC available power and the battery SOC) and the variation of load conditions with its predetermined priority level, then the PMRC impels to curtail the lesser level priority load sequentially.

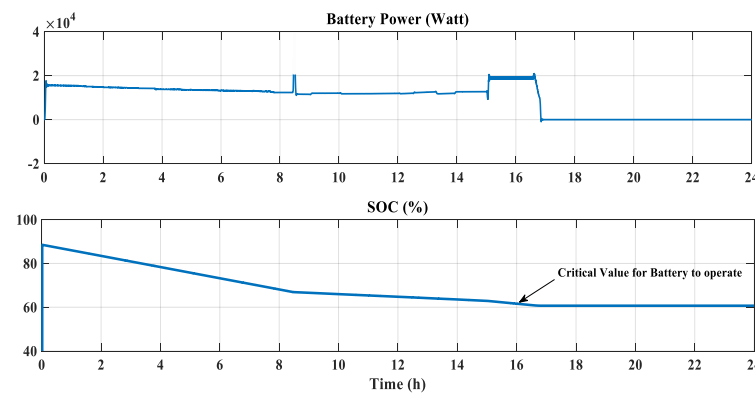
Without applying DSM, as depicted in Fig. 11.a, according to ZWZR there is a low generated power from the hybrid RES that is not able to totally supply the load profile, however the FC power can supply the load with the assistance of battery units. The initial SOC of the battery units was at SOC_{max} of 90% and then decreases with the full utilization till reaching the predetermined critical limit of operation ($SOC_{min_critical} = 60\%$) at $t = 16:00$. As expected, the no. of battery cycles here for discharging events over the whole day, as illustrated in Fig. 11.b, is low compared to Day 1 (EPPS mode) and thus the aging of the battery will be slower. Here the PMRC algorithm checks the availability of the reserve power of hybrid ESS to supply the variations of loads and if that reserve of power is not sufficient, sequential curtailments will take place according to the predetermined priority level in Table 1. It starts by the air conditioning load for the villages (L4-3A) then L4-2A then L4-1A with low priority levels: 9, 8 and 7) from $t = 2:00$ till 5:00 passing by the lighting & service loads for villages (L4-3B then L4-2B then L4-2B with moderate priority levels: 6, 5 and 4) at $t = 6:00$ to 9:00 as shown in the last graph of Fig. 12.

The third graph of Fig. 12 describes the variation of L3 (services for the police station & the bank with priority level: 3) till the full curtailment at $t = 13:45$ whenever the SOC is below than the nominal value of 70% and the capacity of the reserve power in hybrid ESS is not sufficient to supply total loads at this time.

As depicted in the second graph of Fig. 12, the heavy load industries (L2-1, L2-2), which have the highest priority, are kept supplied in this mode although their consumed power is gradually increasing. But at time $t = 16:30$, as the SOC reaches the $SOC_{min_critical}$, the food and packaging industry (L2-3) is cut off for a certain period to maintain the sustainability for the most critical loads represented by the hospital (L1), the steel and the cement industries (L2-1, L2-2) from $t = 16:30$ to 24:00 as illustrated in Fig. 12, at this while in order to preserve the lifetime and the capacity Ah limit of batteries, it is recommended for batteries to be entirely switched off, while the FC remaining power is responsible for supplying the rest of loads as illustrated in the Fig. 11.b.



(a) Power trends including wind power, PV power, battery and FC with total load profile



(b) Output battery power and corresponding SOC

Fig. 11: Generated and consumed power with the battery performance through Day 4 covering scenario No. 4 (ZWZR) without DSM

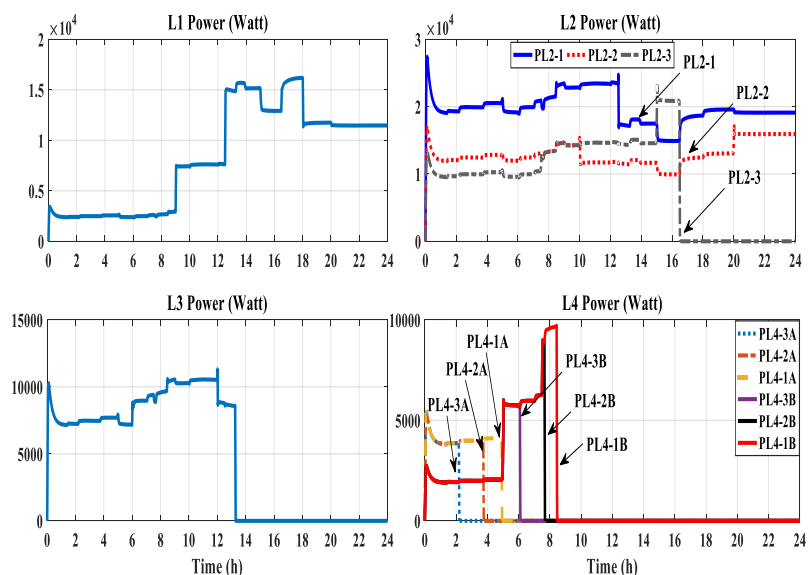


Fig. 12: Detailed L1, L2, L3 and L4 profile variation through Day 4 covering scenario No. 4 (ZWZR) without DSM

4.5 Results for LSM mode at Day 4 covering scenario No. 4 (ZWZR) when applying DSM

Some of the pre-described DSM strategies are also implemented for Day 4 (ZWZR) to estimate the improvement of load sustainability while minimizing end-users consumption costs. According to Eq. (12) and (13), the minimum selected shifting factor, applied on some of the aforementioned shiftable loads, is considered by $S_{Lmin}(t) = 0.8$. The load shifting and energy conservation strategies that can be followed by some of the pre-described loads contribute in reducing power

consumption compared to the same loads without applying DSM at the same day are described in Table 4. It summarizes the peak load demands with and without applying DSM strategies for the four loads and the peak load reduction. It also demonstrates the curtailment time duration with and without DSM. It can be observed that implementing DSM strategies reduces the peak load demand for each load. Actually, however that the PMRC algorithm verifies LSM mode for that day and sequential curtailment of loads are occurred, but Fig. 13 ensures that the loads are more sustainable for greater time intervals over that day when applying DSM strategies.

Table 4: Load sustainability with and without DSM through Day 4 covering scenario No. 4 (ZWZR)

Area	Load Serial	Priority Level	Without DSM		With DSM			
			Peak Load (kW)	Load Curtailment Duration	Peak Load (kW)	Load Curtailment Duration	Peak Reduction (kW)	Percentage Reduction (%)
Hospital	L1	1	15.6	0	8.0	0	7.6	48.7
Industries	L2-1	1	49.0	0	46.0	0	3	6.12
	L2-2	1		0				
	L2-3	2		7 h and 30 min.		3 h and 30 min.		
Police and Bank	L3	3	10.50	10 h and 15 min.	8.15	7 h	2.35	22.38
Tourist Villages	L4-1A	4	17.27	19 h	12.20	15 h	5.07	29.35
	L4-2A	5		20 h		16 h and 30 min.		
	L4-3A	6		22 h		18 h and 30 min.		
	L4-1B	7		15 h and 30 min.		9 h		
	L4-2B	8		16 h and 30 min.		12 h		
	L4-3B	9		18 h		13 h		

As the simulation results confirm that the proposed DSM strategies have succeeded in substantially decreasing the peak load demand, considerable cost savings are achieved for the tested Day No. 4, which may be repeated for three months over the year. To estimate such cost saving, the electricity cost should be considered, which is varied over time daily and seasonally. To study the economic benefit of the integrated EMS with DSM penetration in the proposed system, the electricity cost data is extracted from Nord Pool website [39] to get the average daily cost for days 25th - 28th of January 2019 as given in Fig. 14. Therefore, the total electricity cost of the microgrid load without applying DSM strategy is estimated by \$ 8807.299 for 90 days with the worst case scenario (ZWZR) similar to Day 4 (28th of December 2017) that is repeated seasonally over the year; whereas such operating cost will decrease to only \$7292.37 when applying DSM strategies, resulting in 17.2% saving in cost.

microgrids with large scale loads. In such case, it is expected to give better simulation results for both cost saving and load sustainability especially when the study is implemented for complete year.

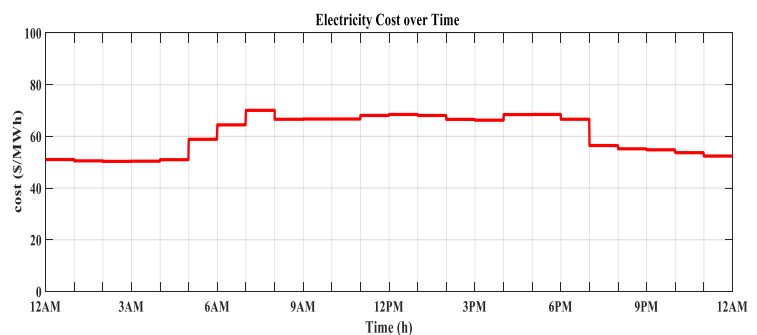


Fig. 14 Hourly cost data (average for 25th - 28th January 2019) [39]

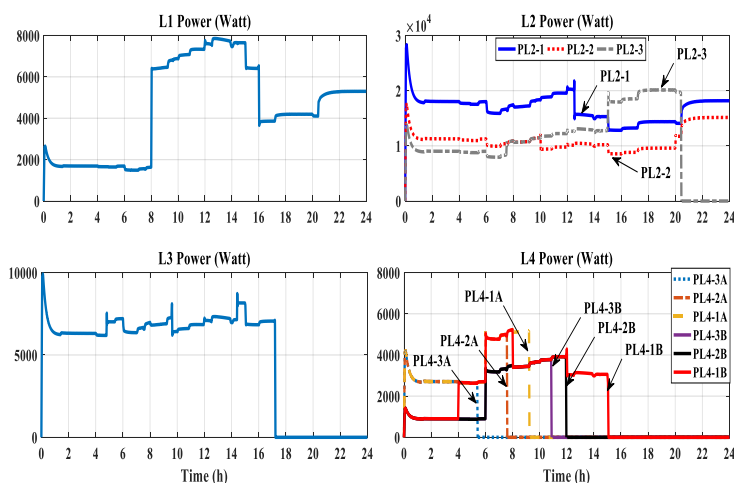


Fig. 13: Detailed L1, L2, L3 and L4 profile variation through Day 4 covering scenario No. 4 (ZWZR) with applying DSM

Meanwhile, it is worth mentioning that the growth of controllable loads with large scale values results in increasing the net savings of consumer costs, moreover the study for the DSM strategies over the whole year ensures more gross savings. The DSM strategies were applied based on a day-ahead load shifting, valley filling and energy conservation strategies and thus can be generalized for large

4.6 Results for the battery lifetime estimation

As previously discussed, the value of discharge current has significant effect on battery aging. This impact is evaluated in Eq. (6) and Eq. (7), it requires the battery data such as the depth of discharge vs. number of cycles, current vs. capacity and discharge pattern, *i.e.* the discharge current vs. discharge time. The charge and the discharge pattern events for the Li-ion battery are simulated for all dominant weather scenarios: HWHR, MWMR, LWMR and ZWZR taken into consideration that these tested scenarios cover the whole year and the project lifetime is about 20 years. Based on SAFT Company technical specification [33], the Intensium Max Li-ion battery is selected as one of the most convenient type of batteries for such microgrid projects, the calendar lifetime is greater than 25 years at normal operating conditions of 25 °C which is suitable for Zaafarana site as the average recorded temperature for the studied year was 19 °C, while the minimum and maximum recorded temperature was 6 °C and 42 °C respectively. Table 5 summarizes the estimated loss of battery life in years for each scenario based on its simulation results and the pre-described battery performance.

Table 5 Battery loss of life estimation in years for each scenario

Weather Scenario	PMRC Mode of operation	Estimated battery loss of life (years)
High wind/High radiation (HWHR) over 3 months	EPPS	3.28
Medium wind/Medium radiation (MWMR) over 3 months	EPPS	1.99
Low wind/Medium radiation (LWMR) over 3 months	LCM	2.77
Zero wind/Zero radiation (ZWZR) over 3 months	LSM	0.8
Overall operation over a year		8.84

Actually each weather scenario is repeated for around 90 days/year, as depicted in Table 5, for example the HWHR scenario in the EPPS mode reduces in the calendar lifetime of battery about 3.28 years and the total operation of the four scenarios in a year reduces the calendar lifetime of the battery about 8.84 years. Since the original calendar lifetime of battery is about 25 years so the estimated battery lifetime in a complete year of operation for cumulative possible modes of operation is reduced to about 16.16 years which clarifies that the regular replacement for such a battery will be within around three years during the lifetime of the project. Such results are in full agreement with studies [40], [41] that consider batteries replacement within two or three years. However, combining two batteries with diesel generation as in [42], the replacement of the Li-ion batteries is improved to three times in project lifespan. Recently, it may be recommended to extend and improve the lifetime of battery by combining other types of storage systems with battery such as two battery units as in [41] or when utilizing a battery-supercapacitor-hybrid storage system as proposed in [43-45].

4.7 Summarizing Dynamic Operating System States for Three Tested Days

As discussed before, the proposed PMRC generates the proper operation system states based on the scenario of input weather data, load profile and actual limitations of all subsystems. Fig. 15 summarizes the achieved system states along the 24 hours for three simulated days. As shown, Day 1 represents EPPS mode (states 1 to 3), while Day 3 characterizes LCM in state 4. LSM is illustrated (states 5 to 9) for Day 4 when either DSM is applied or not. As shown, a seamless mode transfer between the three modes of operation is verified.

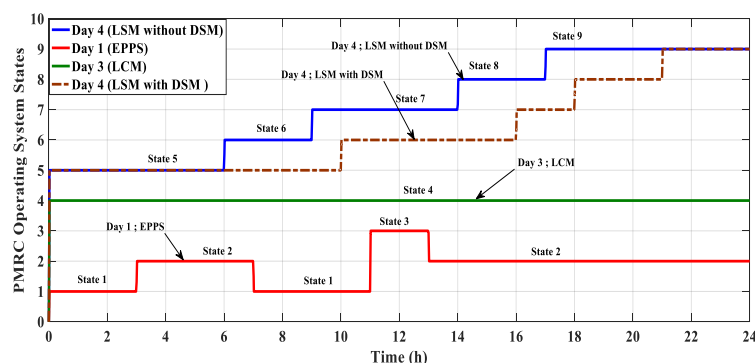


Fig. 15: Operating system states for Day 1, 3 and 4

5. Conclusion

A power management and control strategy for a hybrid RES and hybrid ESS microgrid operates as standalone in a remote area is presented. Coordination and exchanging between the available and the reserve power of the two renewable energy sources based on an integrated EMS with DSM using two-level control based on MAS is proposed. An online central dynamic EMS is achieved with realistic data for a typical year analysis to achieve load requirements. The performance of the proposed control strategy is evaluated under different weather scenarios HWHR, MWMR, LWMR and ZWZR.

The PMRC generates three modes of operation EPPS, LCM and LSM. The EPPS and LCM are two effective operating modes in achieving load sustainability while the LSM is achieved based on both limits of battery *SOC* and the hydrogen pressure of the FC. LSM is implemented according to the priority level for loads.

As the batteries are the most expensive part of microgrids, estimating battery lifetime for the all possible modes of operation has been also verified for further EMS enhancement. Based on the battery discharge patterns, the possible weather scenarios in a year have reduced the calendar lifetime of battery by 8.84 years resulting in regular replacement for such a battery within three years during the lifetime of the project.

Several DSM strategies based on load shifting, valley filling and energy conservation are presented under complete system contingency scenario which represents three months a year. Such strategies result in peak demand reduction and 17.2% electricity consumption saving besides better load availability for the curtailed loads in the LSM. Thus, the proposed PMRC with the corporation of the DSM strategies offers an obvious advantage as it can prevent the system from totally blackouts in the event of either the uncertainty of renewable sources conditions or inadequate energy reserves.

References

- [1] Access to electricity www.iea.org/sdg/electricity/. (Standards and Reports)
- [2] M.-S. Lu, C.-L. Chang, W.-J. Lee, and L.Wang, "Combining the wind power generation system with energy storage equipment", *IEEE Trans. Ind. Appl.*, vol. 45, no. 6, pp. 2109-2115, Nov./Dec. 2009. (Article)
- [3] P. K. Goel, B. Singh, S. S. Murthy, and N. Kishore, "Isolated wind-hydro hybrid system using cage generators and battery storage", *IEEE Trans. Ind. Electron.*, vol. 58, no. 4, pp. 1141-1153, Apr. 2011. (Article)
- [4] T. Zhou and B. François, "Energy management and power control of a hybrid active wind generator for distributed power generation and grid integration", *IEEE Trans. Ind. Electron.*, vol. 58, no. 1, pp. 95-104, Jan. 2011(Article).
- [5] N. Gyawali and Y. Ohsawa, "Integrating fuel cell/electrolyzer/ultracapacitor system into a stand-alone microhydro plant", *IEEE Trans. Energy Convers.*, vol. 25, no. 4, pp. 1092-1104, Dec. 2010. (Article)
- [6] C. Wang and M. H. Nehrir, "Power management of a stand-alone wind/ photovoltaic/fuel cell energy system", *IEEE Trans. Energy Convers.*, vol. 23, no. 3, pp. 957-967, Sep. 2008. (Article)
- [7] A. Hajizadeh, M. A. Golkar, and A. Feliachi, "Voltage control and active power management of hybrid fuel-cell/energy-storage power conversion system under unbalanced voltage sag conditions", *IEEE Trans. Energy Convers.*, vol. 25, no. 4, pp. 1195-1208, 2010. (Article)
- [8] S. D. G. Jayasinghe, D. M. Vilathgamuwa, and U. K. Madawala, "Direct integration of battery energy storage systems in distributed power generation", *IEEE Trans. Energy Convers.*, vol. 26, no. 2, pp. 977-685, June 2011. (Article)
- [9] Allahviridzadeh, Yousef, Mustafa Mohamadian, and Mahmoud-Reza Haghi Fam, "Study of energy control strategies for a standalone PV/FC/UC microgrid in a remote area", *International Journal of Renewable Energy Research (IJRER)*, vol. 7.3, pp. 1495-1508, 2017 (Article).
- [10] T. Zhou, B. Francois, M. el H. Lebbal, and S. Lecoeuche, "Real-time emulation of a hydrogen-production process for assessment of an active wind-energy conversion system", *IEEE Trans. Ind. Electron.*, vol. 56, no. 3, pp. 737-746, Apr. 2009. (Article)
- [11] Dou C, Liu B and Guerrero, "Event-triggered hybrid control based on multi agent system for microgrids", *IET Gener. Transm. Distrib.*, vol. 8, no. 12, pp. 1987-1997, June 2014. (Article)
- [12] Dou X, Quan X, Wu Z, Hu M, Yang K, Yuan J and Wang M, "Hybrid multi agent control in microgrids: framework, models and implementations based on IEC 61850", *Energies*, vol. 8, no. 1, pp. 31-58, May 2014. (Article)
- [13] T.K.A. Brekken, A.Yokochi, A. von Jouanne, Z. Z.Yen, H. M. Hapke, D. A. Halamay "Optimal energy storage sizing and control

- for wind power applications”, *IEEE Trans. Sustain. Energy*, vol. 2, no. 1, pp. 69-77, Apr. 2011. (Article)
- [14] Kotra, S., and Mishra, M. K., “Energy management of hybrid microgrid with hybrid energy storage system”, *4th International Conference on Renewable Energy Research and Applications (ICRERA)*, Palermo, Italy, pp. 856-860, 22-25 Nov. 2015. (Conference Paper)
- [15] Jun, M. A., and Mustafa Baysal, “Online Energy Management Strategy Based On Adaptive Model Predictive Control For Microgrid With Hydrogen Storage”, *International Journal of Renewable Energy Research (IJRER)*, vol. 8.2, pp. 861-870, 2018.(Article)
- [16] E. Muljadi and H. Ed. Mc Kenna, “Power quality issues in a hybrid power system”, *IEEE Trans. Ind. Appl.*, vol. 38, no. 3, pp. 803-809, May/June 2002. (Article)
- [17] Y. Zhang, A. A. Chowdhury, and D. O. Koval, “Probabilistic wind energy modeling in electric generation system reliability assessment”, *IEEE Trans. Ind. Appl.*, vol. 47, no. 3, pp. 1507-1514, May/June 2011. (Article)
- [18] Enrico Telaretti, Mariano Ippolito and Luigi Dusonchet, “A simple operating strategy of small-scale battery energy storages for energy arbitrage under dynamic pricing tariffs”, *Energies*, vol. 9, no. 1, Dec. 2015. (Article)
- [19] L. Dusonchet, M.G. Ippolito, E. Telaretti, G. Zizzo and G. Graditi, “An optimal operating strategy for combined res-based generators and electric storage systems for load shifting applications”, *4th IEEE International Conference on Power Engineering, Energy and Electrical Drives (POWERENG)*, Istanbul, Turkey, 21 Oct. 2013. (Conference Paper)
- [20] Eric Hittinger, Ted Wiley, John Kluza and Jay Whitacre, “Evaluating the value of batteries in microgrid electricity systems using an improved energy systems model”, *Energ. Convers. Manage.*, vol. 89, no. 4, pp. 458-472, Jan 2015. (Article)
- [21] Amir-Sina Hamed and Abbas Rajabi-Ghahnavieh, “Explicit degradation modelling in optimal lead-acid battery use for photovoltaic systems”, *IET Gener. Transm. Distrib.*, vol. 10, no. 4, pp. 1098-1106, Mar. 2016. (Article)
- [22] “Review of Strategies and Technologies for Demand Side Management on Isolated Mini Grids,” M. Harper, 2013. (Standards and Reports)
- [23] Roy, A., Auger, F., Bourguet, S., Dupriez-Robin, F. and Tran, Q. T., “Benefits of Demand Side Management strategies for an island supplied by marine renewable energies”, *7th International Conference on Renewable Energy Research and Applications (ICRERA)*, Paris, France, pp. 474-481, 14-17 Oct. 2018. (Conference Paper)
- [24] A. Oudalov, and A. Timbus C. Yuen, “The provision of frequency control reserves from multiple micro-grids”, *IEEE Trans. Ind. Electron.*, vol. 58, no. 1, pp. 173-183, Jan. 2011. (Article)
- [25] Load statistics www.cced.gov.eg/ar/(Standards and Reports).
- [26] Modern-Era Retrospective analysis for Research and Applications, windspeed, Temperature and solar radiation data, www.soda-pro.com/web-services/meteo-data/merra. (Standards and Reports)
- [27] Wind speed extrapolation, Roughness according to European Wind Atlas. websites.pmc.ucsc.edu/~jnoble/wind/extrap/. (Standards and Reports)
- [28] Sim Power Systems, Reference, Hydro-Québec, MathWorks, Inc. Natick, MA, 2016.
- [29] K. Kumai, Y. Kobayashi, H. Miyashiro, N. Terada, T. Iwahori, et al., “Cycle Life Estimation of Lithium Secondary Battery by Extrapolation Method and Accelerated Aging Test”, *J Power Sources*, vol. 97-98, pp. 697-701, July 2001. (Article)
- [30] H. Wakaki, K. Saito, T. Shodai and A. Yamashita, “Capacity Estimation and Lifetime Expectancy of Large-Scale Nickel Metal Hydride Backup Batteries”, *27th International Telecommunications Conference (INTELEC 05)*, Berlin, Germany, 18-22 Sept. 2005. (Conference Paper)
- [31] T.Y. Tasi, C.W. Chuang, W.B. Shr and C.C. Hua, “Design and Implementation of a Residual Capacity Estimator for Lead-Acid Batteries”, *2nd Conference on Industrial Electronics and App.*, Harbin, China, 23-25 May 2007. (Conference Paper)
- [32] B.L. Johnson and S. Drouilhet, “A Battery Life Prediction Method for Hybrid Power Applications”, *35th AIAA Aerospace Sciences Meeting and Exhibit*, pp. 6-9, Reno, Nevada January 6-9, 1997. (Article)
- [33] SAFT Batteries website <https://www.saftbatteries.com/products> (Standards and Reports).
- [34] X. Tang, B. Liu, and F., “State of charge estimation of LiFePO4 battery based on a gain-classifier observer”, *Energy Procedia*, vol. 105, pp. 2071-2076, May 2017. (Article)
- [35] T. O. Akinbulire, P. O. Oluseyi, and O. M. Babatunde, “Techno-economic and environmental evaluation of demand side management techniques for rural electrification in Ibadan, Nigeria”, *Int. J. Energy Environ. Eng.*, vol. 5, no. 4, pp. 375-385, Aug. 2014. (Article)
- [36] A. Saengprajak, “Efficiency of demand side management measures in small village electrification systems,” PhD Thesis, Kassel University press, ISBN: 978-3-89958-273-4, 2007. (Article)
- [37] Palma-Behnke, Rodrigo, Benavides, Carlos, Aranda, et al., “Energy management system for a renewable based microgrid with a demand side management mechanism”, *IEEE Symposium on Computational Intelligence Applications In Smart Grid (CIASG)*, Paris, France, 11-15 April 2011. (Conference Paper)
- [38] SolarWorld, “The Solar2World program of SolarWorld AG”. (Standards and Reports)
- [39] Dayahead prices, www.nordpoolgroup.com/Market-data1/Dayahead/AreaPrices. (Standards and Reports)
- [40] Jun Xiao, Linqun Bai, Fangxing Li, Haishen Liang and Chengshan Wang, “Sizing of Energy Storage and Diesel Generators in an Isolated Microgrid Using Discrete Fourier Transform (DFT)”, *IEEE Trans. Sustain. Energy*, vol. 5, no. 3, pp. 907-916, July 2014. (Article)
- [41] Zifa Liu, Yixiao Chen, Ya Luo, Guankun Zhao and Xianlin Jin, “Optimized Planning of Power Source Capacity in Microgrid, Considering Combinations of Energy Storage Devices”, *Appl. Sci.*, vol. 6, no. 12, pp. 379-416, Dec. 2016. (Article)
- [42] Mitchell Lee, Daniel Soto and Vijay Modi, “Cost versus reliability sizing strategy for isolated photovoltaic micro-grids in the developing world”, *Renew. Energ.*, vol. 69, pp. 16-24, Sep. 2014. (Article)
- [43] Anthony M. Gee, Francis V. P. Robinson and Roderick W. Dunn, “Analysis of Battery Lifetime Extension in a Small-Scale Wind-Energy System Using Supercapacitors”, *IEEE Trans. Energy Convers.*, vol. 28, no. 1, pp. 24-33, March 2013. (Article)
- [44] Gaetani-Liseo, M., Alonso, C., & Jammes, B., “Impacts of supercapacitors on battery lifetime in hybrid energy storage system in building integrated photovoltaic DC micro-grid”, *7th International Conference on Renewable Energy Research and Applications (ICRERA)*, Paris, France, pp. 1247-1252, 14-17 Oct. 2018. (Conference Paper)
- [45] Abeywardana, D. B. W., Hredzak, B. and Agelidis, V. G., “Battery-supercapacitor hybrid energy storage system with reduced low frequency input current ripple”, *4th International Conference on Renewable Energy Research and Applications (ICRERA)*, Palermo, Italy, pp. 328-332, 22-25 Nov. 2015. (Conference Paper)